Available online at www.sciencedirect.com
ScienceDirect
International Journal of Heat and Mass Transfer 51 (2008) 3113–3126
International Journal of HEAT and MASS TRANSFER
www.elsevier.com/locate/ijhmt

A three-dimensional thermal-fluid analysis of flat heat pipes

Bin Xiao, Amir Faghri *

Department of Mechanical Engineering, University of Connecticut, 261 Glenbrook Road, Unit 2337, Storrs, CT 06269, United States

Received 14 July 2007; received in revised form 21 August 2007
Available online 22 October 2007

Abstract

A detailed, three-dimensional model has been developed to analyze the thermal hydrodynamic behaviors of flat heat pipes without empirical correlations. The model accounts for the heat conduction in the wall, fluid flow in the vapor chambers and porous wicks, and the coupled heat and mass transfer at the liquid/vapor interface. The flat pipes with and without vertical wick columns in the vapor channel are intensively investigated in the model. Parametric effects, including evaporative heat input and size on the thermal and hydrodynamic behavior in the heat pipes, are investigated. The results show that, the vertical wick columns in the vapor core can improve the thermal and hydrodynamic performance of the heat pipes, including thermal resistance, capillary limit, wall temperature, pressure drop, and fluid velocities due to the enhancement of the fluid/heat mechanism form the bottom condenser to the top evaporator. The results predict that higher evaporative heat input improves the thermal and hydrodynamic performance of the heat pipe, and shortening the size of heat pipe degrades the thermal performance of the heat pipe.

1. Introduction

Flat heat pipes are an efficient technology for electronics and spacecraft cooling applications due to their high thermal conductivity, reliability, and low weight penalty [1]. With the development of PC technology, a flat-plate type heat pipe called "vapor chamber" has been used as an advanced heat dissipation device for high performance computers in the recent years due to its low thermal resistant and adaptable structure [2]. A flat heat pipe is an enclosed chamber whose inner surfaces are lined with a capillary wick structure with the remaining volume containing the vapor. The working fluid is vaporized by an external heat source at the evaporator, the generated pressure difference drives vapor from the evaporator to the condenser, where it condenses and enters into wick structures. The capillary pressure in the wick pumps the condensed liquid back to the evaporator for vaporization. This internal phase-change circulation will continue as long as flow passage is not blocked and sufficient capillary pressure is maintained.

Experimental investigations on flat heat pipes have been conducted by some researchers. Wang and Vafai [3] performed an experimental investigation of the transient characteristics of a flat heat pipe during start-up and shutdown operations. The effects of input power and the heat transfer coefficient on the thermal performance of the heat pipe were investigated. The results indicated that the wick in the evaporator section provides the largest resistance to the heat transfer process, followed by the wick in the condenser section. It was found that the heat transfer coefficient has an insignificant effect on the maximum temperature difference on the outside surfaces of the flat heat pipes. The experimental results were compared with the analytical results and were found to be in very good agreement. Xuan et al. [4] experimentally and numerically studied the performance and mechanisms of a flat heat pipe in which a layer of sintered copper powder is applied to the heated surface of the heat pipe. They experimentally measured the performance of the heat pipe by varying the heat fluxes, orientations, and amount of the working fluid. Haddad et al. [5] has conducted experimental measurements of

* Corresponding author. Tel.: +1 860 486 0419; fax: +1 860 486 5088.
E-mail address: amir.faghri@uconn.edu (A. Faghri).

0017-9310/$ - see front matter © 2007 Elsevier Ltd. All rights reserved.
doi:10.1016/j.ijheatmasstransfer.2007.08.023

Nomenclature

f	friction factor
h	enthalpy (J/kg)
h_{fg}	latent heat of vaporization (J/kg)
H	height of the heat pipe (m)
$\mathbf{I}$	identity matrix
$\mathbf{K}$	permeability tensor (m^2)
L	length of the heat pipe (m)
$\dot{m}''$	evaporative mass flux (kg/s m^2)
$\mathbf{n}$	unit normal vector
p	pressure (Pa)
Q	heat input (w)
t	time (s)
$\mathbf{t}$	unit tangential vector
ΔT	change in temperature (K)
T	temperature (K)
u	x-velocity (m/s)
v	y-velocity (m/s)
$\mathbf{v}$	volume-averaged velocity (m/s)
V	elementary volume (m^3)
$\mathbf{V}$	velocity vector (m/s)
w	z-velocity (m/s)
W	width of the heat pipe (m)
Δx	distance a section spans (m)
x	Cartesian or axial coordinate (m)
y	Cartesian coordinate (m)
z	Cartesian coordinate (m)

Greek symbols

ε	emmisivity
φ	porosity
h	heat transfer coefficient (W/m^2 K)
μ	dynamic viscosity (N s/m^2)
ρ	density (kg/m^3)
σ	Stefan–Boltzmann constant
$\boldsymbol{\tau}$	stress tensor (N/m^2)
Φ	viscous dissipation (watts/m^3)

Subscripts

c	cooled section, condenser, coolant
f	fluid
h	heated section, evaporator
e	referring to evaporative heat input
l	liquid
m	center of a heated or cooled section
s	solid
v	vapor
w	wick

the performance of mini flat heat pipes with square sides of 45×45 mm and thickness of 3 mm. The results showed that the flat heat pipe with sintered wick material performed significantly better than solid copper at high heat fluxes, and heat pipe orientation has minimal effect. On the other hand, the heat pipe with a mesh wick showed a degraded performance of the heat pipe at high heat fluxes. They also conducted Flotherm CFD analysis on the temperature distributions of the heat pipes. Machiroutu et al. [6] utilized DOE (Design of Experiments) to understand the parametric effects on performance by thermal resistance analysis and developed some simple rules to optimize the design of flat heat pipes.

In order to better reveal the physical mechanism of heat pipes for the optimization of product design, mathematical physical modeling has been developed to investigate flat heat pipes designed in the recent years. Most one-dimensional analytical and numerical models focus on heat transfer performance and various limitations, especially the capillary limit in flat micro miniature heat pipes. Khrustalev and Faghri [7] developed a one- dimensional model for flat heat pipes with triangular grooves. The maximum heat transfer restricted by capillary limit was predicted. The agreement between the numerical solution and experimental data of Plesh et al. [8] was reasonably good. Longtin et al. [9] solved a one-dimensional model of a flat micro heat pipe, yielded pressure, velocity and film thickness along the length of the pipe. Interfacial and vapor shear stress terms have been included in the model. The results implied that the short, wide pipes can get high heat transport capability. Lefevre and Lallemand [10] presented an analytical solution for liquid and vapor flows as well as the temperature inside a flat micro heat pipe. Maximum heat transfer capability was also calculated.

Multidimensional models have been developed for simulation of flat heat pipes in the past decades. Ooijen and Hoogendoorn [11] presented a steady two-dimensional numerical analysis of the vapor core in a horizontal flat heat pipe. The vapor flow patterns under different radial Reynolds numbers were illustrated and compared with a porous plate model. Koito et al. [12] carried out numerical analyzes on start-up heat transfer characteristics of the flat heat pipes. Heat conduction was considered in the liquid-wick region and a lumped analysis was applied in the vapor region. The results revealed the thermal responses for sudden change in heat flux and compared the numerical results with the authors' experimental results. Koito et al. [13] showed a steady-state, three-dimensional model of the flat heat pipe with three regions of a solid wall, liquid-wick and the vapor chamber. They assumed that the vapor flow is laminar and the vapor condenses and liquid evaporates only at the interface between the vapor and liquid-wick regions. The heat transfer in solid wall and the liquid wick regions were taken as a pure heat conduction problem. The results showed that the temperature gradient near the heat source was comparatively large, while the temperature at

the top of the heat pipe was almost uniform. Contrary to the wick column, the copper column was found to enhance the heat transfer above the heat source. The results revealed the heat transfer characteristics of the vapor chamber, which were hardly affected by the heat source position.

Zhu and Vafai [14] developed a steady, incompressible, three-dimensional numerical model for an asymmetrical flat heat pipe to reveal the vapor flow in the vapor channel as well as liquid flow in the wick. All wicks were assumed to be isotropic and saturated with wetting liquid. The transport properties of the fluid were assumed to be constant. The vapor injection and suction rates were assumed to be uniform on the top and bottom wicks and negligible on the vertical wicks. The results were compared and agreed with the analytical solution. It was found that the transverse pressure variations had an insignificant effect on the vapor flow. Vadakkan et al. [15] numerically analyzed the transient and steady-state performance of a flat heat pipe subjected to heating with multiple discrete heat sources. Three-dimensional flow and energy equations are solved in the vapor and liquid regions, along with conduction in the wall. Saturated flow models were used for heat transfer and fluid flow through the wick. Rice and Faghri [16] developed a numerical model to investigate the screen wick of cylindrical/flat heat pipes with single and multiple heat sources as well as constant, convective and radiative heat sinks. The prediction of the maximum capillary pressure under a given heating load and the capillary dry-out limitations were conducted in their simulations. For additional literature about experimental investigation and numerical simulations in the flat heat pipes, one can refer to [17–21].

In this work, a complete three-dimensional model has been developed to analyze thermal/fluid characteristics and capillary limit in the flat heat pipes without empirical correlations. The governing equations for the wall, wick and vapor cores are derived and solved by SIMPLE algorithm. The objective of the present work is to investigate the sensitivity of the evaporative heat input, the vertical wick columns in the vapor chamber, and the size of the heat pipe to the temperature distribution, pressure drop, and fluid dynamics in the heat pipes.

2. Mathematical modeling

A schematic diagram of a flat heat pipe with vertical wick columns is presented in Fig. 1. The flat heat pipe consists of three parts: the wall of the heat pipe; the porous wicks saturated with working fluid; and the vapor channel. A heat source is input on the top surface center of the heat pipe. Vapor flows downward and condenses at the vapor/wick interfaces by releasing latent heat of vaporization. The vertical wick blocks in the vapor channel provide a return mechanism for the condensate when liquid transports from the bottom wicks to the top wicks. The basic assumptions are as follows:

1. The vapor flow is assumed to be laminar and incompressible, and the density change of vapor is predicted by the ideal gas state equation.
2. The wicks are assumed to be saturated with wetting fluid and the transport properties of the fluid are assumed to be constant.

This steady-state model is based on the numerical solution of the governing equations for mass, momentum, and energy in the two phases, the equations of thermodynamic equilibrium at the vapor/wick interface, and the conduction equation of the wall. Because of the asymmetry of the investigated flat heat pipe, the mathematical model will be calculated in a quarter domain as illustrated in Fig. 1.

2.1. Vapor core

The steady, compressible continuity equation in the vapor channel is:

$$\nabla \cdot \rho \mathbf{V} = 0. \tag{1}$$

The momentum equation for the vapor flow is:

$$\nabla \cdot (\rho \mathbf{V}\mathbf{V}) = -\nabla p + \nabla \cdot \boldsymbol{\tau} \tag{2}$$

where the stress tensor, $\boldsymbol{\tau}$, is:

$$\boldsymbol{\tau} = \mu(\nabla \mathbf{V} + \nabla \mathbf{V}^T) - \frac{2}{3}\mu(\nabla \cdot \mathbf{V})\mathbf{I}. \tag{3}$$

The energy equation in the vapor channel can be written as:

$$\nabla \cdot (\rho \mathbf{V} h) = \nabla \cdot (k \nabla T) + \Phi \tag{4}$$

where Φ is the viscous dissipation:

$$\Phi = \nabla \mathbf{V} : \boldsymbol{\tau}. \tag{5}$$

The density change of the vapor flow by pressurization is calculated by the ideal gas law,

$$\rho = \frac{p}{RT}. \tag{6}$$

The ideal gas constant, R, is the universal gas constant divided by the molecular weight.

2.2. Wicks

Under the assumption of the saturated, incompressible, steady-state liquid flow in the wicks, the mass balance in the wicks is described by the volume-average method [22],

$$\nabla \cdot \varphi \langle \mathbf{V} \rangle_{\mathrm{f}} = 0. \tag{7}$$

When the momentum equation is volume-averaged, the viscous interaction between the fluid and the solid matrix can be modeled by Darcy's Law and an inertial drag term, the momentum equation becomes:

$$\nabla \cdot (\varphi \rho \langle \mathbf{V} \rangle_{\mathrm{f}} \langle \mathbf{V} \rangle_{\mathrm{f}}) = -\varphi \nabla p + \mu \nabla^2 \langle \mathbf{V} \rangle_{\mathrm{f}} - \frac{\mu}{\mathbf{K}} \varphi^2 \langle \mathbf{V} \rangle_{\mathrm{f}} - \frac{f}{\mathbf{K}^{1/2}} \rho \varphi^3 |\langle \mathbf{V} \rangle_{\mathrm{f}}| \langle \mathbf{V} \rangle_{\mathrm{f}}. \tag{8}$$

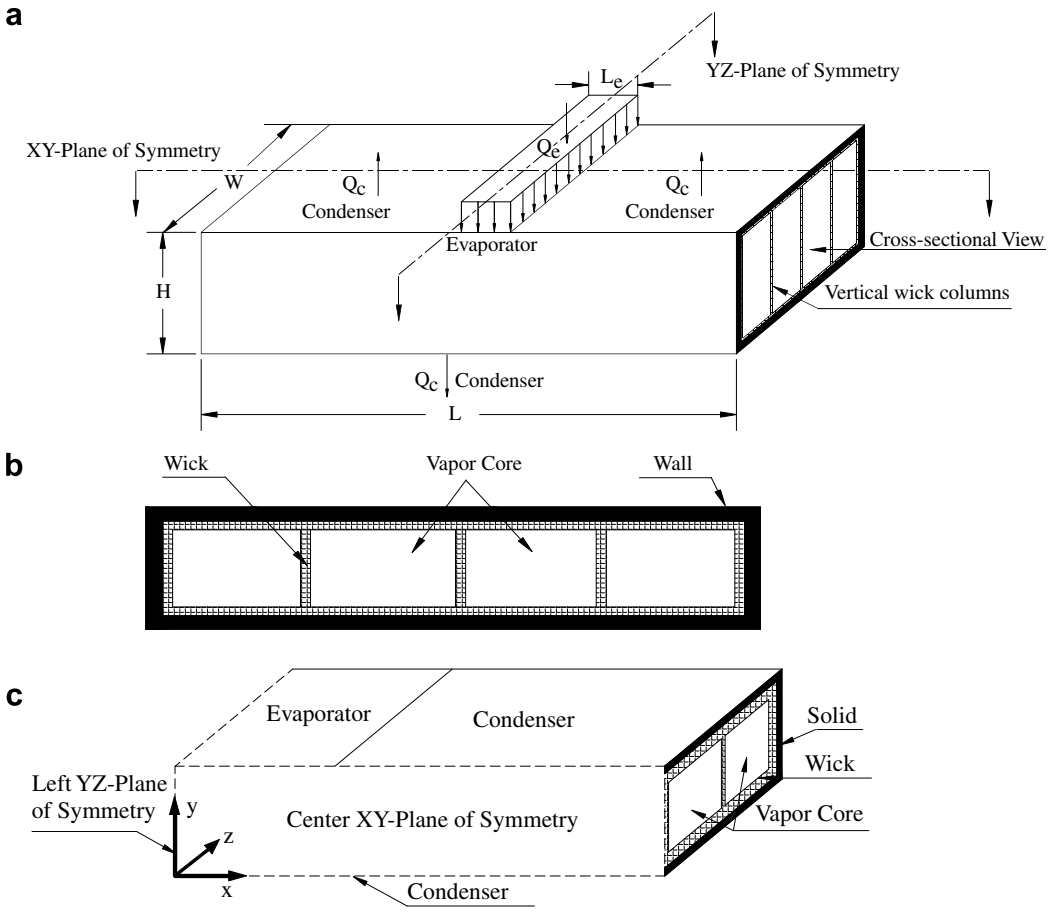

Fig. 1. Schematic diagram of the flat heat pipe: (a) geometry of the heat pipe; (b) cross-sectional view in *YZ* plane; and (c) computational domain.

The volume-averaged energy equation in the wicks is:

$$\nabla \cdot (\varphi \rho \langle \mathbf{V} \rangle_f \langle h \rangle_f)_l = \nabla \cdot k_{eff} \nabla \langle T \rangle \tag{9}$$

where,

$$(\rho h)_{eff} = \varphi (\rho h)_f + (1-\varphi)(\rho h)_s \tag{10}$$

$$k_{eff} = \frac{k_f (k_f + k_s - (1-\varphi)(k_f - k_s))}{k_f + k_s + (1-\varphi)(k_f - k_s)}. \tag{11}$$

2.3. Solid wall

The steady-state energy balance in the solid wall is determined by heat conduction:

$$\nabla \cdot (k \nabla T) = 0. \tag{12}$$

2.4. Wick/vapor interface

The conservation of mass at the wick/vapor interface is:

$$\dot{m}'' = -\rho_v \mathbf{V}_v \cdot \mathbf{n}_v = \varphi \rho_l \langle \mathbf{V}_l \rangle_f \cdot \mathbf{n}_l. \tag{13}$$

The mass flux is determined by the energy balance at the interface:

$$\dot{m}'' = (-k_{eff} \nabla T \cdot \mathbf{n}_w - k_v \nabla T \cdot \mathbf{n}_v)/h_{fg}. \tag{14}$$

Because the enthalpy of both the liquid and the vapor is already included in the latent heat of vaporization, the sensible heat is not included in the above equation. The tangential velocity of the vapor is zero at the interface because of the interaction with the solid wick. Also, the only component of the liquid velocity at the wick/vapor interface is assumed normal to the interface, therefore,

$$\mathbf{V}_v \cdot \mathbf{t} = \langle \mathbf{V}_l \rangle_f \cdot \mathbf{t} = 0. \tag{15}$$

With the assumptions of liquid-saturated wicks and stationary interface, the local normal momentum equation at the interface is:

$$p_v - p_l - \dot{m}''(\mathbf{V}_l - \mathbf{V}_v) = \frac{2\sigma_{lv}}{r_{eff}} = p_c. \tag{16}$$

The interfacial temperature is equivalent to the saturation temperature which is calculated by the Clausius–Clapeyron equation:

$$T_I = T_{l,I} = T_{v,I} = T_{sat} = \left(\frac{1}{T_0} - \frac{R}{h_{fg}} \ln \left(\frac{P_v}{P_0} \right) \right)^{-1} \tag{17}$$

where the saturation temperature is based on the vapor pressure at the wick/vapor interface and the wick/vapor interface is assumed to have no thickness. Therefore, the liquid and vapor temperatures are both equal to the saturation temperature. Also, all of the components of velocity in the wick are zero at the interface between the outer wall and the wick:

$$\mathbf{V} = 0. \tag{18}$$

2.5. Other interfaces

At the top center of the heat pipe $\left(y = H, \frac{L-L_e}{2} \leqslant x \leqslant \frac{L+L_e}{2}, 0 \leqslant Z \leqslant W\right)$, a constant heat flux is applied:

$$k_s \nabla T \cdot \mathbf{n}_s = \frac{Q_e}{WL_e} \tag{19}$$

where $\mathbf{n}_s$ is the unit normal vector, pointing out of the solid wall.

At the outer wall of the condenser sections $(y = H, \left|x - \frac{L}{2}\right| > \frac{L_e}{2}, 0 \leqslant Z \leqslant W)$ and $(y = 0,\ 0 \leqslant x \leqslant L,\ 0 \leqslant Z \leqslant W)$, the convective boundary condition is:

$$-k_s \nabla T \cdot \mathbf{n}_s = h(T - T_\infty) \tag{20}$$

where $\mathbf{n}_c$, is the unit normal vector, pointing into the solid wall. The outer section that is not heated or cooled is adiabatic:

$$\nabla T \cdot \mathbf{n}_s = 0. \tag{21}$$

At the interface between the outer wall and the wick, the thermal boundary condition is:

$$-k_s \nabla T \cdot \mathbf{n}_s = k_{\text{eff}} \nabla T \cdot \mathbf{n}_w. \tag{22}$$

The end caps of the heat pipe are adiabatic in the outer wall, wick and vapor sections:

$$\nabla T \cdot \mathbf{n}_{s,w,v} = 0. \tag{23}$$

In the vapor channel and the wicks, the velocity is zero at the end caps:

$$\mathbf{V}_v = \langle \mathbf{V}_l \rangle_f = 0. \tag{24}$$

The boundary conditions at the planes of symmetry are:

$$\mathbf{V} \cdot \mathbf{n} = 0 \tag{25}$$

$$\nabla \mathbf{V} \cdot \mathbf{t} \cdot \mathbf{n} = 0. \tag{26}$$

2.6. Numerical solutions

A finite volume approach is used to discretize the governing equations. A staggering scheme is applied to interpolate the pressure in the same manner as a staggered mesh. The hydrodynamic and energy equations are coupled and solved iteratively. The SIMPLE algorithm developed by Patankar [23] is used to introduce velocity–pressure coupled relations into the governing equations. A power-law scheme is implemented for the convective flux and diffusion flux. The discretized equations are solved by a line-by-line TDMA. The overall numerical procedure for the investigated problem is:

1. Specify geometric dimensions, thermophysical properties, initial conditions, and boundary conditions in the interfaces.
2. Solve the wall heat conduction equation.
3. Solve the momentum and energy equations for liquid flow.
4. Calculate the vapor density using the ideal gas equation.
5. Solve the pressure-correction equation to obtain the vapor velocity and pressure.
6. Calculate the vapor temperature based on the vapor pressure using the Clausius–Clapeyron equation.
7. Repeat steps 2–6 until converged results are obtained.

3. Results and discussions

3.1. Model validation

In order to validate the present model, the numerical solutions are compared with the experimental results from work by Wang and Vafai [3], in which the physical dimensions of the heat pipe are taken as 190.50 mm in length, 139.70 mm in width and 34.93 in height. The copper wall of the heat pipe is 3.175 mm thick. The porous wicks are made of sintered copper powder and the thickness is 1.651 mm. The heater is 139.70 mm in length and 50.8 mm in length. The initial temperature throughout the heat pipe is 285 K and the heat transfer coefficient of the condenser is 1230 $\text{W/m}^2\,\text{K}$. The thermophysical properties of the heat pipe wall, wick, and vapor core are given in Table 1. Fig. 2 shows a comparison of the numerical results with the experimental data for the temperature distributions at the surface of the top and bottom walls of the flat heat pipe. As can be seen from the figure, the experimental data and numerical results are reasonably close. The deviation in the condenser section in the top wall is mainly due to the variation of the convective heat transfer coefficient dependent of different surface temperature in the experiment, which is assumed to be constant in the numerical model. The grid size used in the calculation domain is $59 \times 23 \times 48$. A meshing independence test is conducted by doubling the grid size. On average, the deviation of the results is less than 0.1%.

Table 1
Thermophysical properties of the heat pipe materials and the working fluid

Materials	Parameters	Value
Copper	Thermal conductivity	401 W/m K
	Specific heat	386 J/kg K
	Density	8390 kg/m^2
	Pore radius of the wicks	3.1×10^{-5} m
	Wick permeability	7×10^{-12} m^2
	Wick porosity	0.5
Wick/water	Thermal conductivity	1.7988 W/m K
	Specific heat	4182 J/kg K
	Density	999 kg/m^2
	Viscosity	1.0015×10^{-3} N s/m^2
	Latent heat	2473 kJ/kg
Water vapor	Thermal conductivity	0.0188 W/m K
	Specific heat	1874 J/kg K
	Density	Ideal gas
	Viscosity	8.85×10^{-6} N s/m^2

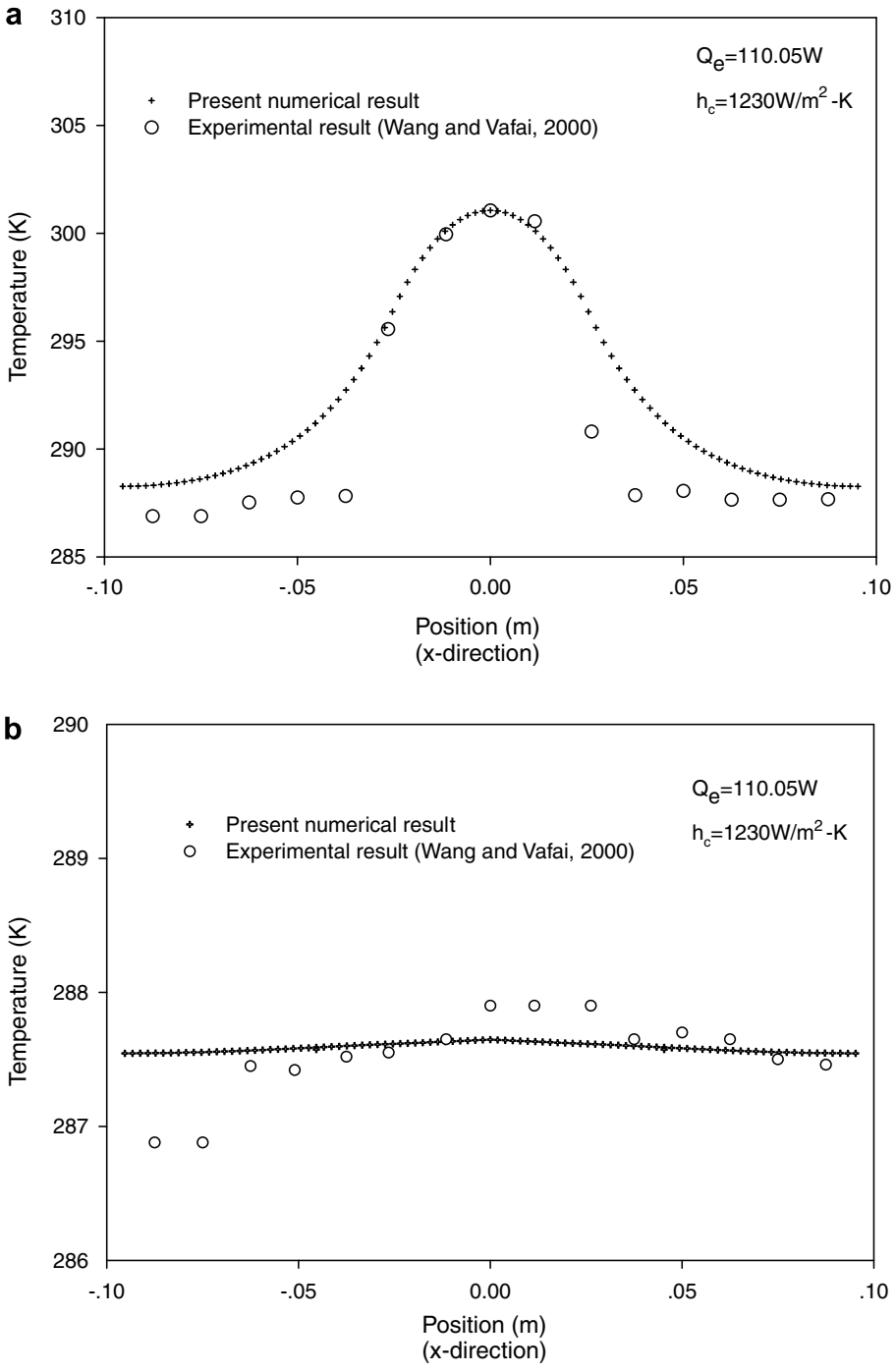

Fig. 2. Verification of numerical results for temperature distribution along a flat heat pipe with vertical wick columns at: (a) the top wall; and (b) the bottom wall at $Z = W/2$.

3.2. Capillary limit

Capillary limit is typically the dominant factor of the various limits that govern the operation of heat pipe. In order to maintain the continuity of interfacial evaporation, the total pressure drop in the heat pipe must be less than or equal to the maximum capillary pumping pressure. If the pore diameter in the wick is insufficient to generate the required capillary pressure, the heat pipe will dry out for the given heat flux. The maximum capillary pressure and corresponding heat transport capacity of a flat heat pipe can be determined by [1],

$$p_{\mathrm{c,max}} = \frac{2\sigma\cos\alpha}{r_{\mathrm{c}}} \tag{27}$$

$$Q_{\max} = \frac{2\sigma\cos\alpha}{L_{\mathrm{eff}} r_{\mathrm{c}}} \cdot \left[\frac{2(fRe)_{\mathrm{v}}\mu_{\mathrm{v}}}{\rho_{\mathrm{v}} D_{\mathrm{h,v}}^2 A_{\mathrm{c,v}} h_{\mathrm{fg}}} + \frac{\mu_{\ell}}{K \rho_{\mathrm{v}} A_{\mathrm{c},\ell} h_{\mathrm{fg}}} \right]^{-1} \tag{28}$$

where r_c is the capillary radius, the effective length of the flat heat pipe and the hydraulic diameter of the vapor core can be expressed as:

$$L_{\text{eff}} = 0.5(L_e + L_c) \tag{29}$$

$$D_{h,v} = \frac{4A_{c,v}}{p_v} \tag{30}$$

where the cross-sectional area of the vapor flow, $A_{c,v}$, as well as the wetted perimeter p_v can be obtained from the derivation by Faghri [1]. The capillary limit calculated by the above equations is 1089.8 W for the heat pipe with vertical wicks by Wang and Vafai [3] and 880.315 W for the corresponding heat pipe without vertical wicks. In order to compare the analytical results with the numerical calculations, the total heat input for the numerical model is decreased from 1200 W and adjusted accordingly until the pressure drop by numerical calculations comes to equal the maximum capillary pressure of the analytical solution, that is, 4.7019×10^3 Pa. The numerical solution predicts that the capillary limit of the heat pipe with vertical wicks is about 1142.56 W, and the capillary limit of the heat pipe

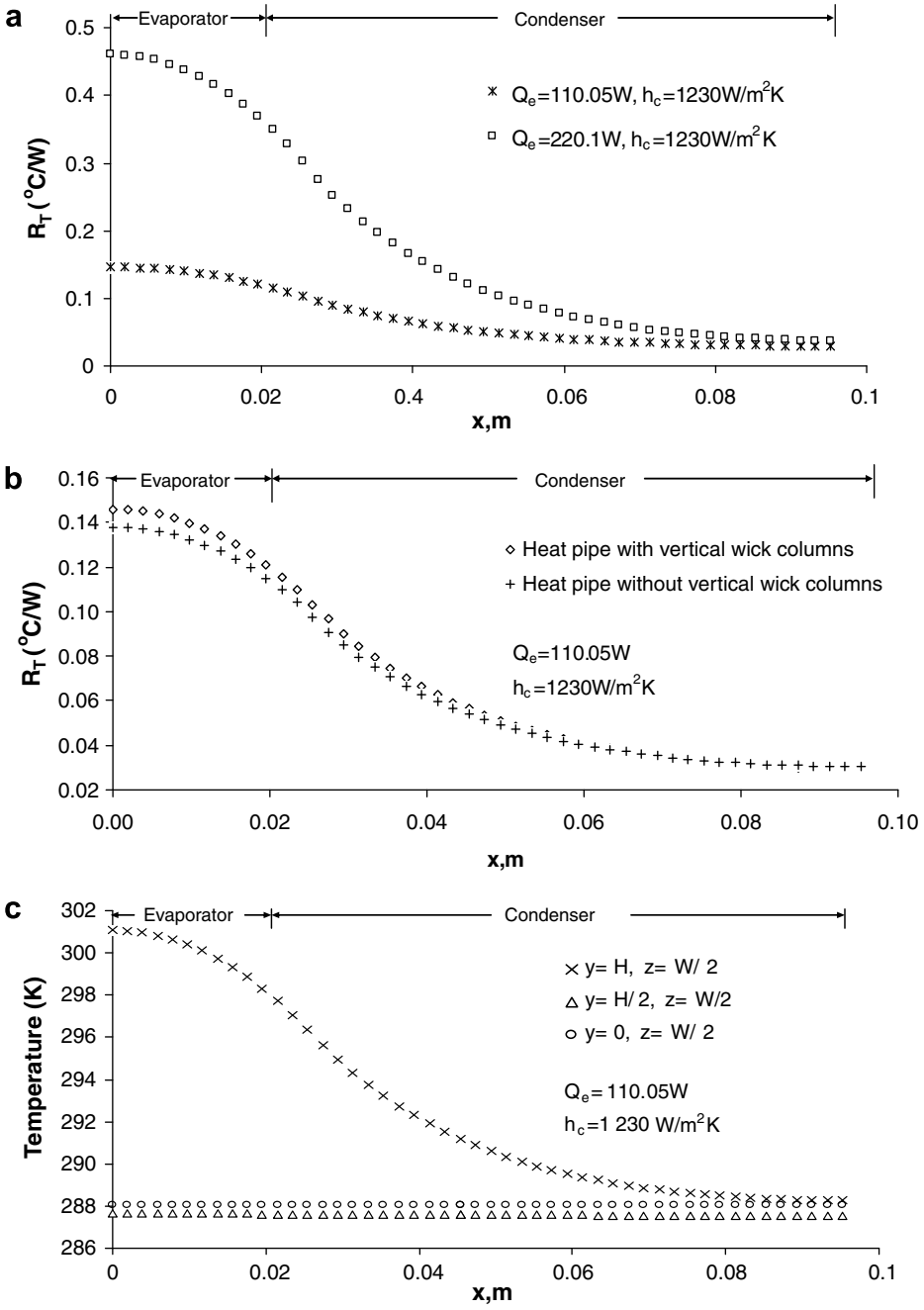

Fig. 3. Thermal characteristics of the flat heat pipe with vertical wicks: (a) effect of heat flux on thermal resistance; (b) effect of vertical wick columns on thermal resistance; and (c) temperature profiles.

without vertical wicks is about 902.36 W. The deviation between numerical and analytical solutions may be caused by the pressure gradient in the numerical calculations, and affected by the mass and heat change at the wick/vapor interface. While in the analytical solution, the effect capillary pressure is assumed to be equivalent to the static capillary pressure.

3.3. Thermal resistance

Thermal resistance is an indication of the heat transfer from the flat heat pipe to the open environment, which is an important concept of the heat pipe design. The thermal resistance from the top wall surface of the flat heat pipe to the ambient environment can be defined as follows [7]:

$$R_T = \frac{T_s - T_a}{Q_e} \tag{31}$$

where T_s is the top wall temperature, T_a is the ambient temperature, and Q_e is the heat dissipation. Fig. 3a and b show the effects of heat flux and vertical wick columns on thermal resistance along the heat pipes. The sharp thermal resistance gradient in the evaporation section is smoothed at the condensation section. As expected, thermal resistance is found to increase significantly around the evaporation section and insignificantly around the condensation section when the heat flux is doubled. As shown in Fig. 3b, the thermal resistance in the flat heat pipe with vertical wick columns is higher than that without vertical wick columns because the vertical wick columns enhance the convective fluid and heat flow in the heat pipes. The temperature profiles at the top wall surface, vapor core and bottom wall surface of the flat heat pipe is illustrated in Fig. 3c. As can be seen, the temperature difference between the top wall surface and vapor core is much larger than between the vapor core and bottom wall surface in the evaporation section. That implies that the wicks in the flat heat pipe contribute the largest resistance to the total heat transfer because of the latent heat releasing in the vapor/wick interface.

3.4. Effect of the vertical wick columns

In order to investigate the geometric parameters that influence the performance of the heat pipe, studies of surface temperature, vapor flow in the core, pressure drop and liquid flow in the wicks in the heat pipe are conducted. Fig. 4 shows the effect of the vertical wicks on the cross-sectional profiles in YZ planes for the vapor velocity vector field in flat heat pipes. The maximum vapor velocity in

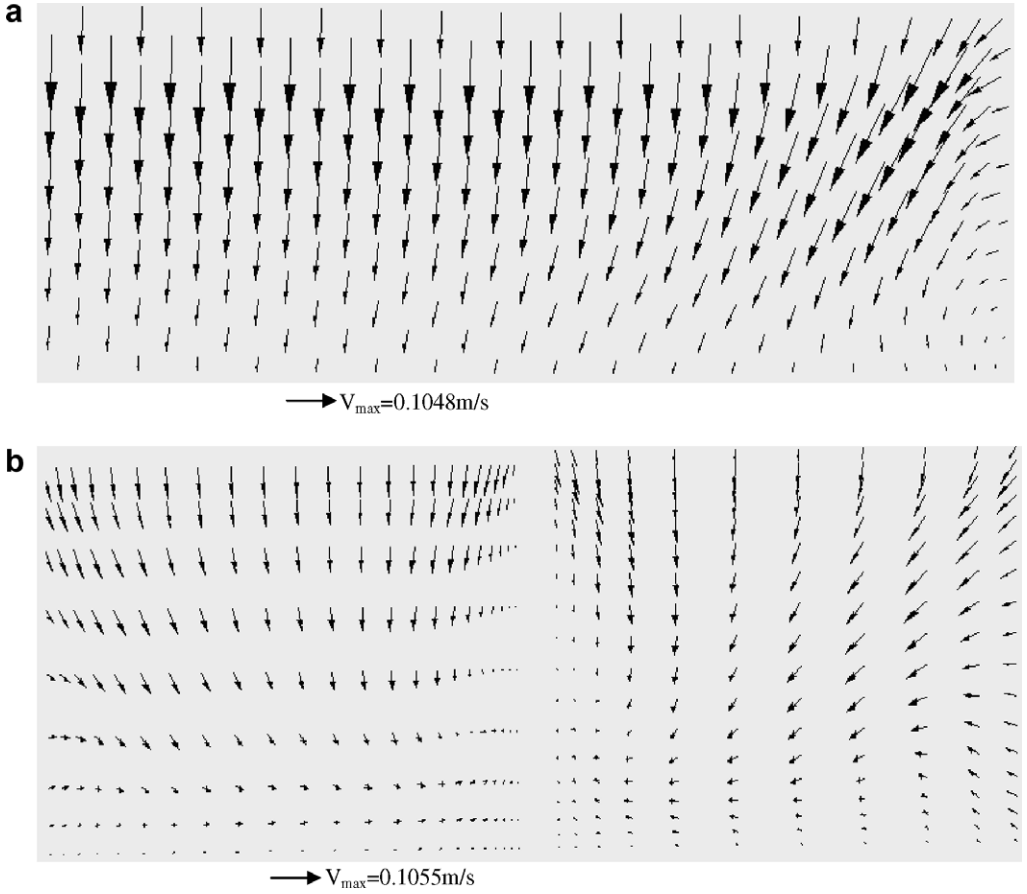

Fig. 4. Effect of vertical wick on the cross-sectional profiles in YZ planes for vapor velocity vector field at $x = 0.1$ L in the flat heat pipes when $Q_e = 110.05$ W, $h_c = 1230$ W/m^2 K: (a) without vertical wick columns; and (b) with vertical wick columns.

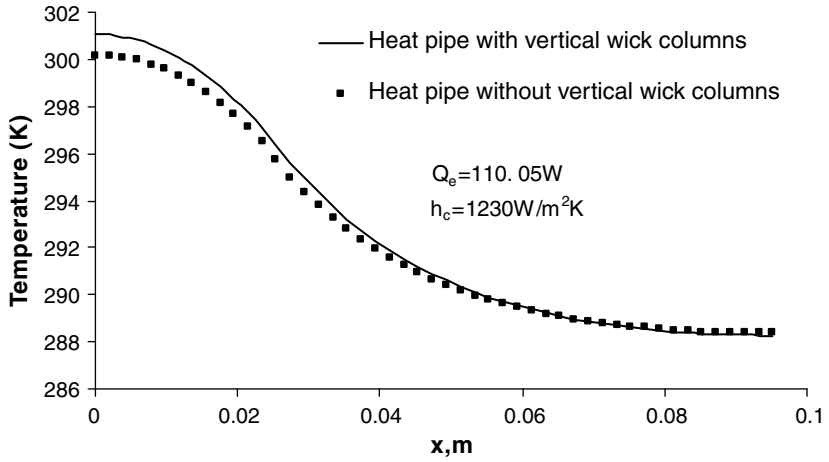

Fig. 5. Effect of vertical wick on the top wall temperature distribution at $z = W/2$ in the flat heat pipes.

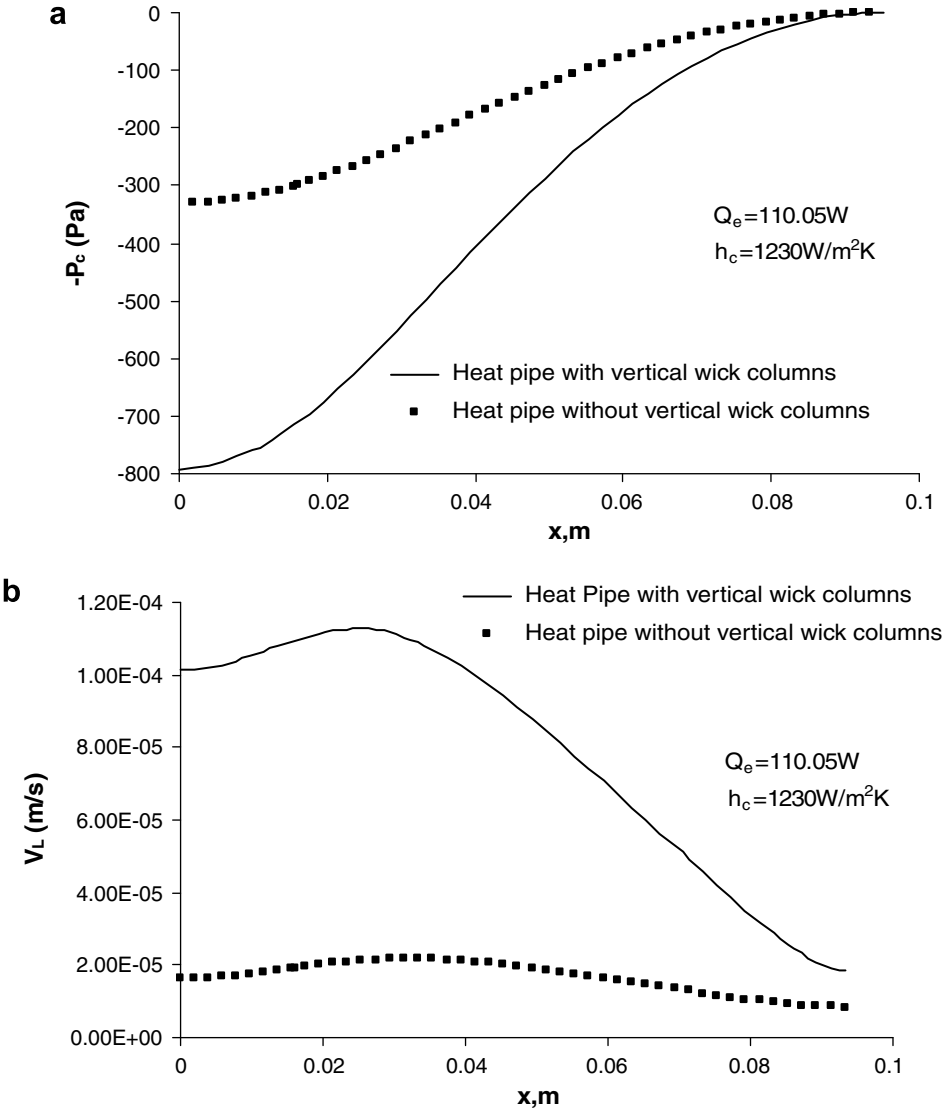

Fig. 6. Effect of vertical wicks on liquid dynamics at $z = W/2$ in the middle of the top wick along the wall: (a) capillary pressure; and (b) liquid velocity.

the vapor core without vertical wick columns is about 0.1048 m/s, the velocities accelerate first and then decelerate in the bottom because of the condensation in the bottom wick/vapor interface. The maximum velocity in the heat pipe with vertical wicks is 0.1055 m/s, a little higher than that in the heat pipe without vertical wicks, due to the increasing vapor pressure caused by the narrowed vapor chamber. Also more horizontal velocities appear in the areas near the edges resulting in a circulation downdream.

Fig. 5 shows the vertical wick effect on top wall temperature distribution at $z = W/2$ in the flat heat pipes. The surface temperature decreases slowly at the evaporator and sharply in the condenser. The maximum temperature at the surface increases with the addition of the vertical wicks. Fig. 6a shows the vertical wick effect on the liquid pressure drop at $z = W/2$ in middle of the top wicks of the flat heat pipes. The maximum pressure drop, which pumps the liquid flow back from the condenser to the evaporator, occurs at the left end of the evaporator. The pressure drop in the heat pipe with the vertical wicks is much higher than the heat pipe without vertical wicks due to the fact that the vertical wick columns in the vapor channel provide an additional return mechanism when liquid transports from the bottom wicks to the top wicks. Fig. 6b shows the vertical wick effect on liquid velocity at $z = W/2$ in the middle of top wicks in the flat heat pipes. The liquid in the wicks accelerates in the condenser zone and decelerates in the evaporator zone because of the condensation and evaporation in the corresponding areas. The average liquid velocity in the wicks is much smaller than the average vapor velocity, since the liquid density is much larger than the vapor density. And the maximum liquid velocity in heat pipes with vertical wick columns is much higher than in those without vertical wick columns, which demonstrates that the vertical wick columns help the liquid transport from the bottom wicks to the top wicks. The above results show that the hydrodynamic and thermal behaviors of the heat pipe are improved with the addition of vertical wick columns. Thus, in the following, the heat pipe with vertical wick columns is chosen to analyze the effects of heat input and the size on the heat pipe performance.

3.5. Effect of heat input

Fig. 7 shows the effect of heat input on the cross-sectional profiles in YZ planes for the vapor velocity vector field in the flat heat pipe. The velocity vector profiles for

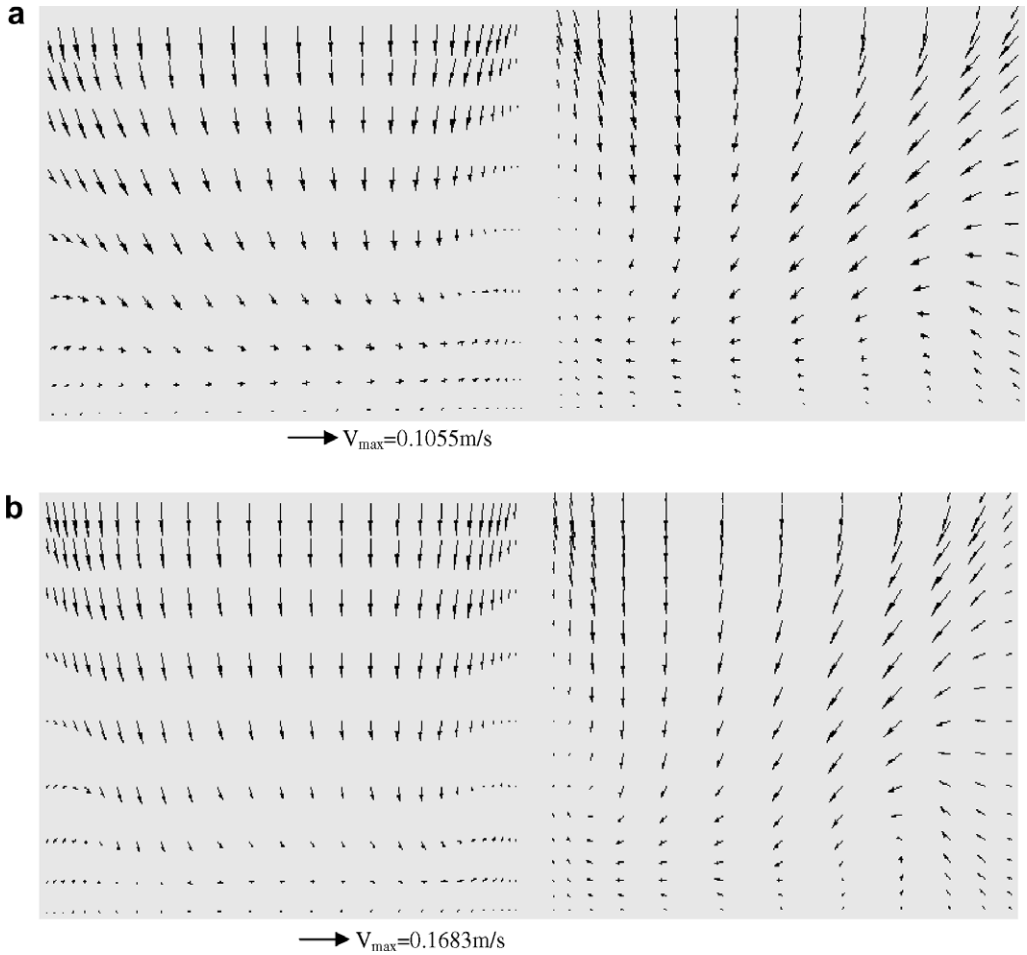

Fig. 7. Effect of heat input on the vapor velocity vector field at $x = 0.1$ L in the flat heat pipe with vertical wicks: (a) $Q_e = 110.05$ W; and (b) $Q_e = 220.1$ W.

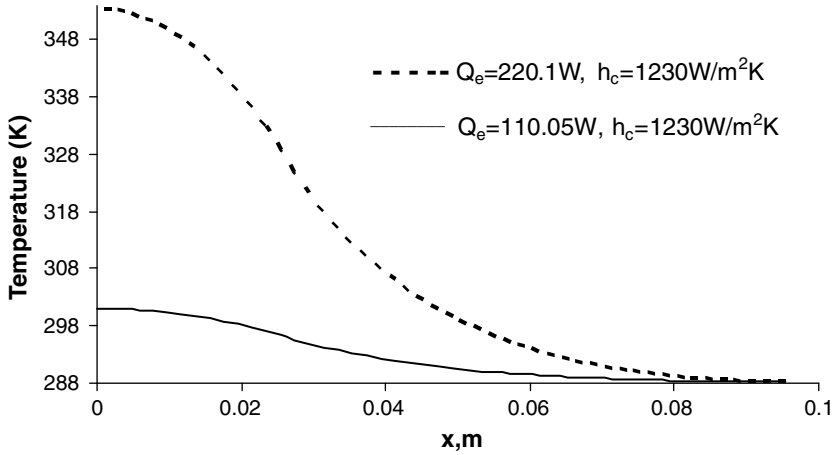

Fig. 8. Effect of heat input on the top wall temperature distribution at $z = W/2$ in the flat heat pipe with vertical wicks.

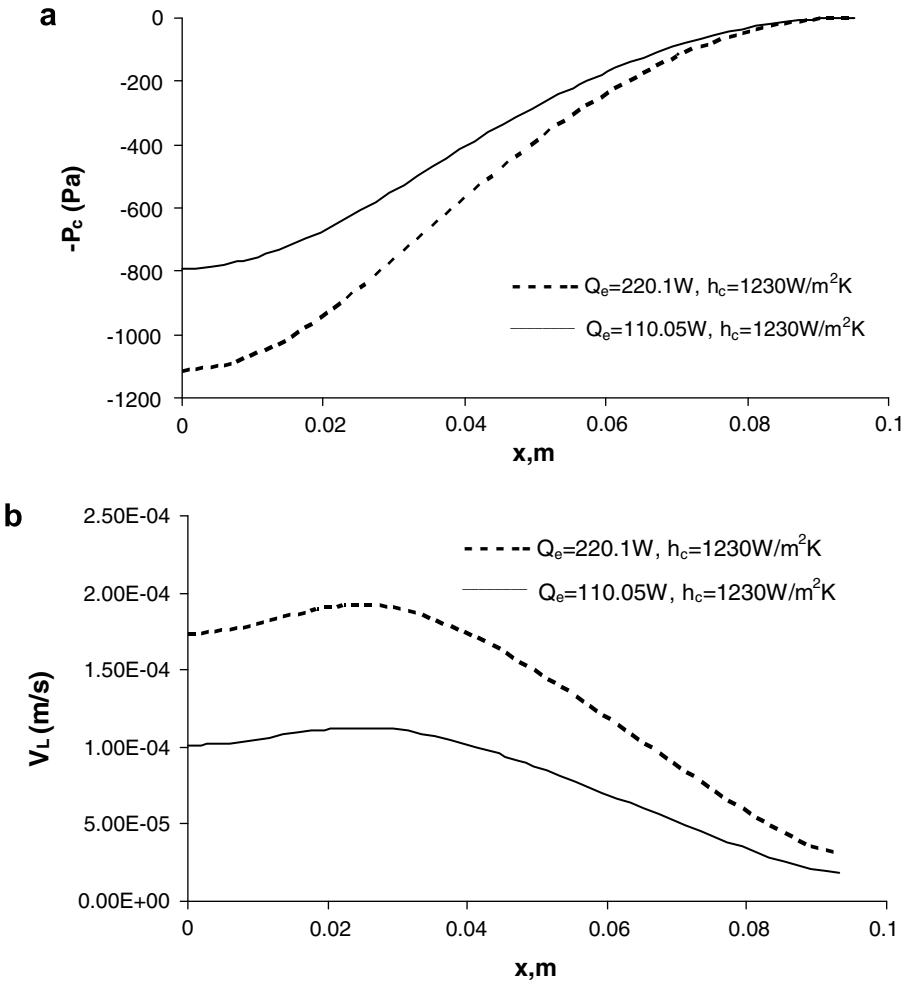

Fig. 9. Effect of heat input on liquid dynamics at $z = W/2$ in the middle of the top wicks along the wall of the flat heat pipe with vertical wicks: (a) capillary pressure; and (b) liquid velocity.

these two cases are similar, but the maximum vapor velocity increases from 0.1055 m/s to 0.1683 m/s because vapor density decreases with higher heat input. Fig. 8 shows the effect of heat input on the top wall temperature distribution at $z = W/2$ in the middle of top wicks of the flat heat pipe with vertical wicks. The temperature increases faster from the condenser to the evaporator and the maximum temperature at the surface increases from about 301 K to 352 K when heat input is doubled. Fig. 9 shows the effect of heat input on liquid dynamics at $z = W/2$ in the middle of top

wicks of the flat heat pipe with vertical wicks. As the mass flow rate increases at the vapor/liquid interface by the increasing condensation of vapor, both the pressure drop and the maximum velocity increase considerably when the heat input increases.

3.6. Effect of heat pipe size

Fig. 10 shows the effect of heat pipe size on the cross-sectional profiles in *YZ* planes for the vapor velocity vector field in the performance of flat heat pipes. The maximum

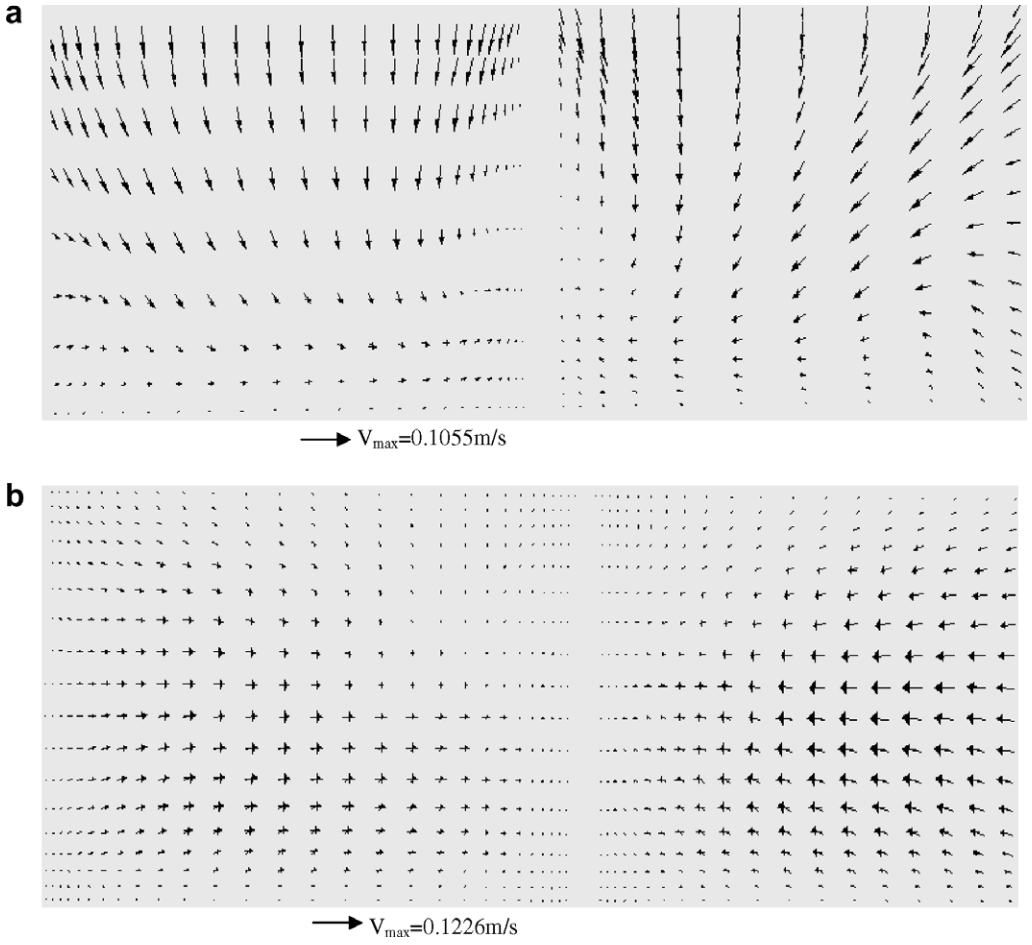

Fig. 10. Comparison of the cross-sectional profiles in *YZ* planes for the vapor velocity vector field at $x = 0.1$ L in the flat heat pipe with vertical wicks: (a) original heat pipe; (b) half size of the original heat pipe.

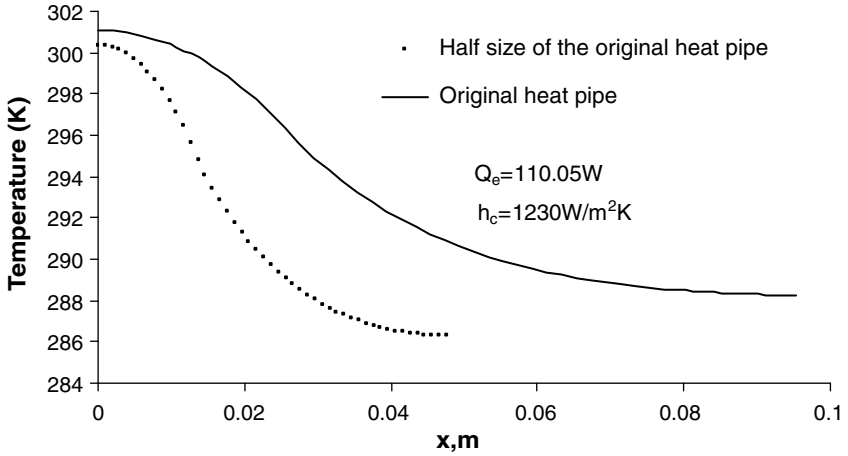

Fig. 11. Effect of size on the top wall temperature distribution at $z = W/2$ in the flat heat pipe with vertical wicks.

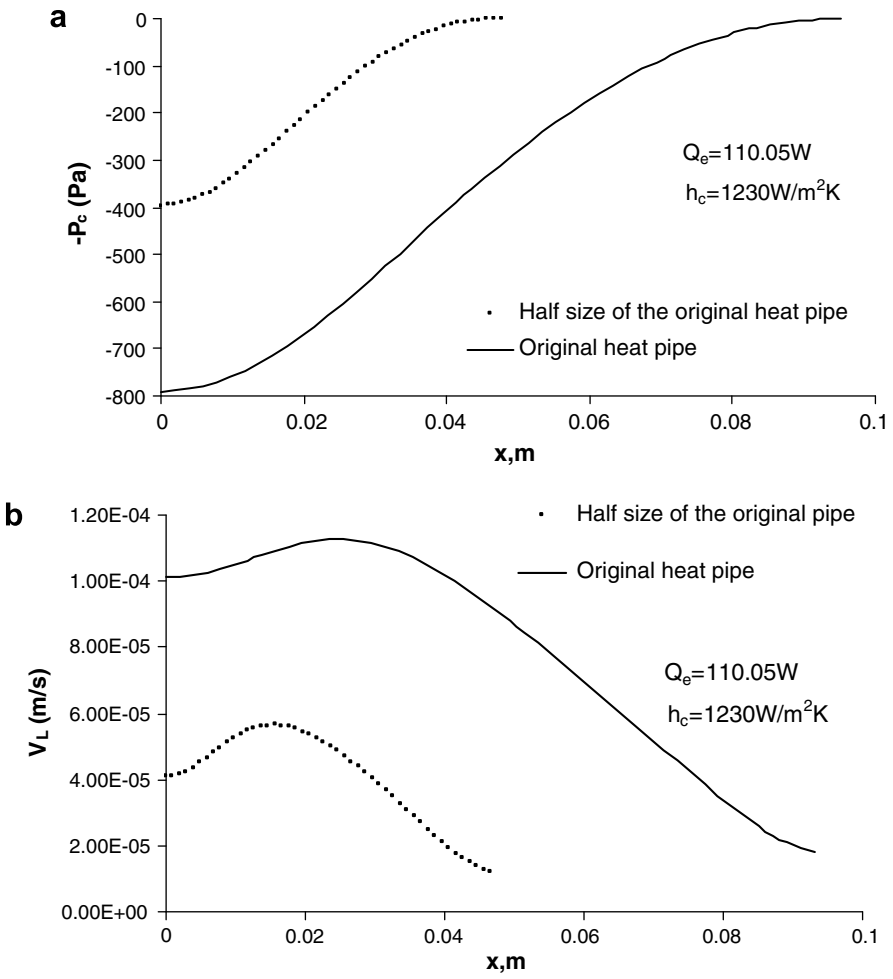

Fig. 12. Effect of heat pipe size on liquid dynamics at $z = W/2$ in the middle of the top wicks along the wall of the flat heat pipe with vertical wicks: (a) capillary pressure; and (b) liquid velocity.

vapor velocity increases from 0.1055 m/s to 0.1226 m/s and horizontal velocities prevail in the heat pipe due to the increasing vapor pressure when the size of the heat pipe is smaller. Fig. 11 shows the effect of heat pipe size on the top wall temperature distribution at $z = W/2$ in the flat heat pipe. Both the maximum and minimum temperatures in the heat pipe decrease with the decreasing evaporative heating area when the size of the heat pipe is shortened. Fig. 12 shows the effect of heat pipe size on the liquid dynamics at $z = W/2$ in the middle of top wicks of the flat heat pipe. Both maximums of the pressure drop and liquid velocity in the heat pipe with half size are less than half values of those in the heat pipes because the decreasing temperature degrades the fluid dynamics in the wicks.

4. Conclusions

A complete, three-dimensional mathematical model without empirical correlations has been developed to analyze the steady-state thermal and hydrodynamic characteristics of flat heat pipes. The model accounts for fluid flow in the vapor chamber and the wicks, heat conduction in the wall, heat and mass transfer at the vapor/wick interface. The numerical analysis determines the capillary limit for the heat transfer capacity and thermal resistance in the heat pipe. Thermal resistance and capillary limit are enhanced with the addition of vertical wick columns in the heat pipes. With the addition of vertical wick columns in the vapor core, the capillary heat transport increases, resulting in higher pressure drops and liquid/vapor velocities, because the vertical wick columns provide a return mechanism for the liquid from the bottom wicks to the top wicks. The results also show that a higher evaporative heat input increases surface temperature, pressure drop, fluid velocities in the wicks and vapor chambers due to the increasing mass flow rate at the vapor/wick interface as vapor velocity increases. The results predict that a larger heat pipe has a better thermal performance than a smaller heat pipe because of the shortened evaporative heating area, although the vapor velocities increase caused by the increasing chamber vapor pressure when the size of the heat pipe is shortened.

References

[1] A. Faghri, Heat Pipe Science and Technology, Taylor and Francis, Washington, DC, 1995.

[2] S. Machiroutu, B. Kluge, M. Kuroda, H. Pokharna, Design and test methodologies of use of heat pipes in laptop PCs, in: The Eighth International Heat Pipe Symposium, Kumamoto University, Kumamoto, Japan, 2006, pp. 229–239.

[3] Y. Wang, K. Vafai, An experimental investigation of the transient characteristics of a flat-plate heat pipe during start-up and shutdown operations, ASME J. Heat Transfer 122 (2000) 525–535.

[4] Y. Xuan, Y. Hong, Q. Li, Investigation on transient behaviors of flat-plate heat pipes, Exp. Therm. Fluid Sci. 28 (2004) 249–255.

[5] A. Haddad, R. Boukhanour, C. Buffone, Testing and simulation of vapor chamber used in electronics cooling, in: The Fourteenth International Heat Pipe Conference, Florianopolis, Brazil, April 22–27, 2007.

[6] M. Mochizuki, Y. Saito, F. Kiyooka, T. Nguyen, X.P. Wu, T. Nguyen, V. Wuttijumnong, Advanced cooling chip by heat pipes and vapor chamber for personal computers, in: The Fourteenth International Heat Pipe Conference, Florianopolis, Brazil, April 22–27, 2007.

[7] D. Khrustalev, A. Faghri, Thermal characteristics of conventional and flat miniature axially-grooved heat pipes, J. Heat Transfer 117 (1995) 1048–1054.

[8] D. Plesch, W. Bier, D. Seidel, K. Schubert, Miniature heat pipes for heat removal from microelectronic circuits, in: Proceedings of the ASME Annual Meeting, Atlanta, GA, 1991.

[9] J.P. Longtin, B. Badran, F.M. Gerner, A one-dimensional model of a micro heat pipe during steady-state operation, ASME J. Heat Transfer 116 (1994) 709–715.

[10] F. Lefevre, M. Lallemand, Coupled thermal and hydrodynamic models of flat micro heat pipes for the cooling of multiple electronic components, Int. J. Heat Mass Transfer 49 (2006) 1375–1383.

[11] V. Ooijen, C.J. Hoogendoorn, Vapor flow calculations in a flat heat pipe, AIAA J. 17 (1979) 1251–1259.

[12] Y. Koito, H. Imura, M. Mochizuki, Transient thermal characteristics of a vapor chamber, in: The Fourteenth International Heat Pipe Conference, Florianopolis, Brazil, April 22–27, 2007.

[13] Y. Koito, M. Komiya, Y. Nakano, H. Imura, M. Mochizuki, S. Torii, A three-dimensional heat transport analysis of a vapor chamber, in: The Eigth International Heat Pipe Symposium, Kumamoto University, Kumamoto, Japan, 2006, pp. 147–152.

[14] N. Zhu, K. Vafai, Vapor and liquid flow in an asymmetrical flat-plate heat pipe: a three-dimensional analytical and numerical investigation, Int. J. Heat Mass Transfer 41 (1998) 159–174.

[15] U. Vadakkan, S.V. Garimella, J.Y. Murthy, Transport in flat heat pipes at high heat fluxes from multiple discrete sources, ASME J. Heat Transfer 126 (2004) 347–354.

[16] J. Rice, A. Faghri, Analysis of screen wick heat pipes, including capillary dry-out limitations, AIAA J. Thermophys. Heat Transfer 21 (3) (2007) 475–486.

[17] M.J. Rightley, C. Tigges, P.R.C. Givler, C.V. Robino, J.J. Mulhall, P.M. Smith, Innovative wick design for multi-source, flat-plate heat pipes, Microelectron. J. 34 (3) (2003) 187–194.

[18] L. Chien, C.C. Chang, Experimental study of evaporator resistance on porous surface in flat heat pipes, in: Inter Society Conference on Thermal Phenomena IEEE, 2002, pp. 1052–1057.

[19] T. Simura, H. Sho, Y. Nakamura, The aluminum flat heat pipe using cyclopentane as working fluid, in: Inter Society Conference on Thermal Phenomena IEEE, 2002, pp. 224–229.

[20] J.B. Chesser, G.P. Peterson, S. Lee, A simplified method for determining the capillary limitation of flat heat pipes in electronics cooling, in: Proceeding of the NHTC '00, Thirty-fourth National Heat Transfer Conference, 2000.

[21] J.Y. Um, L.C. Chow, K. Baker, An experimental investigation of flat heat pipe, Fundamentals of Heat Pipes, vol. 278, ASME HTD, New York, 1994, pp. 21–26.

[22] A. Faghri, Y. Zhang, Transport Phenomena in Multiphase Systems, Elsevier Inc., 2006.

[23] S.V. Patankar, Numerical Heat Transfer and Fluid Flow, McGraw-Hill, New York, 1980.